Boletim da Sociedade Astronômica Brasileira, **34**, no. 1, 7-11
© SAB 2023

The kinetic feedback channel traced by the coronal gas in radio-weak active galactic nuclei

A. Rodríguez-Ardila[1,2], M. A. Fonseca-Faria[1,2]

[1] Laboratório Nacional de Astrofísica - Rua dos Estados Unidos 154, Bairro das Nações. CEP 37504-364, Itajubá, MG, Brazil. e-mail: aardila@lna.br
[2] Divisão de Astrofísica, Instituto Nacional de Pesquisas Espaciais, Avenida dos Astronautas 1758, São José dos Campos, 12227-010, SP, Brazil.

Abstract. The kinetic channel is usually regarded as the dominant feedback process in radio-galaxies. However, its effect in radio-weak AGN is still uncertain and poorly assessed. In this work, we discuss recent results on this matter. In particular, we study the kinetic feedback in a sample of seven radio-weak *bona − fide* active galactic nuclei by means of the high-ionisation gas. We found that the [Fe VII] λ6087 and the [Fe X] λ6374 emission suitably traces this feedback component. Moreover, we show that it extends to distances between 2−3 kpc from the central source, allowing us to set new limits to the size of the coronal line region in AGN. By means of channel maps, we found in all cases that the high-ionisation gas is strongly aligned to the radio-jet and is kinematically perturbed, with splitted line profiles suggesting gas in expansion, decoupled from galaxy rotation. Blue- and red-shifted gas with velocities reaching ∼400 km s^{-1} in excess of the systemic velocity at locations as far as 1 kpc from the AGN are measured. Moreover, the coronal gas morphology and extension coincides with that of the extended X-ray emission, suggesting that it is shock-driven. Models combining the effects of both photoionisation by central source and shocks nicely support this scenario by reproducing the observed emission line strengths of both low- and high-ionisation gas. We derive pre-shock gas densities $n_{\rm H}$ in the range 100−300 cm^{-3}, gas temperatures of up to $T_{\rm e} \sim 3 \times 10^4$ K, and shock velocities of ∼400 km s^{-1}, in agreement to the values derived from the observations. We show that the detection of extended coronal emission probes the presence of the kinetic channel and that it plays a very important role in the feedback energetics, even in radio-weak AGN.

Resumo. O canal cinético é geralmente considerado como o processo de feedback dominante em rádio-galáxias. No entanto, seu efeito em núcleos ativos de galáxia (AGN) radio-fracos ainda é incerto e mal avaliado. Neste trabalho, discutimos resultados recentes sobre o assunto. Em particular, estudamos o feedback cinético em uma amostra de sete AGNs clássicos radio-fracos por meio do gás de alta ionização. Encontramos que as linhas de emissão de [Fe VII] λ6087 e [Fe X] λ6374 descrevem adequadamente essa componente de retro-alimentação. Além disso, mostramos que esse gás se estende até distâncias entre 2−3 kpc da fonte central, permitindo estabelecer novos limites para o tamanho da região de linhas coronais em AGNs. Por meio de mapas de canais, descobrimos que, em todos os casos, o gás de alta ionização encontra-se fortemente alinhado ao jato rádio e é cinematicamente perturbado, com perfis de linhas sugerindo gás em expansão, desacoplado da rotação da galáxia. Observamos gás com velocidades de −400 km s^{-1} a +400 km s^{-1}, em relação a velocidade sistêmica da galáxia, sendo detectada até 3 kpc do AGN. Além disso, a morfologia e a extensão do gás coronal coincidem com as da emissão estendida de raios-X, sugerindo que é esta última é causada por choques. Modelos que combinam os efeitos da fotoionização pela fonte central e choques suportam bem esse cenário, reproduzindo as intensidades das linhas de emissão observadas. Derivamos densidades de gás pré-choque $n_{\rm H}$ na faixa de 100−300 cm^{-3}, temperaturas de gás de até $T_{\rm e} \sim 3 \times 10^4$ K, e velocidades de choque de ∼400 km s^{-1}. Mostramos que a detecção de emissão coronal estendida evidencia a presença do canal cinético e que este desempenha um papel muito importante na retro-alimentação energética, mesmo em AGN rádio-fracos.

Keywords. Galaxies: active – quasars: emission lines – Galaxies: jets – Galaxies: Seyfert – Line: profiles

1. Introduction

The coronal line region (CLR) of active galactic nuclei (AGN) is traditionally regarded as the place where the high-ionisation forbidden lines (i.e., those lines with ionisation potential ≥ 100 eV) are formed (Appenzeller & Wagner 1991). Erkens et al. (1997) conducted the first study aimed at determining the location of the CLR by means of integrated emission line spectra of 15 AGN. They found that the CLR should be compact (< 1″) and located in the innermost portion of the narrow line region (NLR). They also suggested that the highest ionisation gas was involved in outflows because the peak centroid of the coronal lines was very often strongly blueshifted, with the blue wing of the line profiles displaying conspicuous asymmetries. These characteristics were absent in medium and low ionisation lines.

The first systematic study on the extent and morphology of coronal emission in radio-weak AGN using assisted adaptive optics (AO) instruments appeared only in the mid-2000s. Prieto et al. (2005) found extended coronal emission in scales from 30 pc to 200 pc, aligned with the ionisation cone. Later, Rodríguez-Ardila et al. (2006), using seeing-limited spectroscopy studied the spectra of 6 radio-weak AGNs, finding for the first time in the literature, coronal emission with double peak structure in two of these objects (NGC 1068 and NGC 1386). This result associated the coronal lines (CL) to the presence of outflows.

Studies with integral field unit (IFU) spectrographs brought more information about the morphology of the CLR. Müller-Sánchez et al. (2011) and Mazzalay et al. (2013) used AO to spatially resolve the CLR in nearby AGN. They found high-ionisation gas extending between 80 pc to 150 pc from the AGN with signatures of outflows with velocities of up to 1500 km s^{-1}. The velocity field suggested a CLR of biconic morphology. Later, Rodríguez-Ardila et al. (2017) and May et al. (2018) provided with additional examples of extended coronal emission at

spatial scales of a few hundred parsecs and associated to outflows.

Notice that the works above were carried out using data collected with IFUs that have field-of-view (FoV) of $\sim 3'' \times 3''$. Therefore, it was not possible, at that time, to confirm if the coronal gas extends further. Very recently, Rodríguez-Ardila & Fonseca-Faria (2020) reported an extended outflow of high ionised gas in the Circinus Galaxy by means of the CL [Fe VII] λ6087 using the Multi Unit Spectroscopic Explorer (MUSE) at VLT. This result was possible thanks to the much larger FoV, of $1' \times 1'$, of that IFU. The physical conditions of the gas in Circinus show that the extended coronal emission is likely the remnant of shells inflated by the passage of a radio jet.

Very recently, Negus et al. (2021) reported CL emission at kiloparsec-scales from the central source. Their results show CLR reaching out 1.3-23 kpc from the galactic centre, with an average distance of 6.6 kpc. Similar results, pointing out extended CLR at scales of several hundred parsecs were reported by Ramos Almeida & Ricci (2017) in the Teacup galaxy and by Speranza et al. (2022) in the Type-II quasar J0945+1737.

Despite the above results, to the best of our knowledge, no systematic studies of the coronal line extension in nearby sources using IFUs with large field-of-view (FoV), of tens of arcseconds squares, have yet been made. This prompted us to investigate the size of the CLR region in *bona − fide* AGN. We aimed at confirming if it is indeed larger than previously detected, in agreement with the more recent values found in the literature. Moreover, the detection of extended CL emission in AGN is quite important because it traces the footprint of X-ray gas in AGN and therefore, can potentially be used to measure the kinematics of the extended X-ray emission gas (Trindade Falcão et al. 2022).

Thus, taking advantage of the MUSE capabilities, we examine the actual extension of the CLR and its association to the kinetic channel of the feedback in different AGN environments. Here, we analyse a sample of 7 radio-weak, mid- to low-luminosity Seyfert 2 galaxies, with previous report of extended coronal emission at scales of a few hundreds parsecs.

In Sect. 2 we describe our sample and data analysis. In Sect. 3 we characterise the coronal gas extension, geometry and morphology of the CLR as well as the relationship with emission at other wavelength intervals. Sect 4 describes the gas kinematics of the sample. Sect. 5 models the observed extended emission line ratios. Final remarks are in Sect 6. Throughout this work H_0 = 70 km s^{-1} Mpc^{-1}, Ω_m = 0.30, and Ω_{vac} = 0.70, have been adopted.

2. Sample and data analysis

The sample employed in this work is composed of seven local *bona − fide* Seyfert 2 AGN ($z < 0.02$, where z is the redshift), widely known for displaying a low-luminosity radio-jet and a NLR characterised by a bi-conical structure, previously mapped through the [O III] λ5007 emission. They all display [Fe VII] λ6087 in the nuclear spectrum and a NLR that extends to at least 2 kpc from the AGN. Integral Field Unit (IFU) data for The Circinus Galaxy, IC 5063, NGC 1068, NGC 3393, NGC 5643, NGC 5728, and ESO 428-G14 were obtained using MUSE/VLT and retrieved from the European Southern Observatory science portal. The IFU cube for each source is fully reduced, including calibration in flux (in absolute units) and wavelength. Details of the observations and data reduction are provided elsewhere (Mingozzi et al. 2019).

Each data cube was analysed making use of a set of custom PYTHON scripts developed by us as well as software publicly available in the literature. First, we rebinned the cube, reducing the total number of spaxels to $\sim$ 10000. We then removed the stellar continuum across the whole spectral range of MUSE (4700 – 9100 Å) using STARLIGHT (Cid Fernandes et al. 2005) and the Bruzual & Charlot (2003) stellar libraries. This procedure left us with spectra dominated by the nebular emission, allowing us to focus only on the gas emission properties, free of any continuum contamination.

Thereafter, we measured the emission line fluxes of Hα and Hβ at every spaxel on each galaxy to determine the extinction (Galactic and intrinsic) affecting the gas. This was done assuming an intrinsic line ratio Hα/Hβ = 3.1 and the Cardelli et al. (1989) extinction law. All integrated line fluxes measured at each spaxel were corrected by the extinction measured accordingly.

We then constructed maps of the flux distribution for the most important lines such as [O III] λ5007, Hβ, Hα, [Fe VII] λ6087, and [Fe X] λ6374. The analysis of such maps revealed us that the mid- and high-ionised gas is usually arranged in bi-conical structures, with apex at the AGN.

In the following section, we will describe the main results regarding the coronal line extent and morphology of the CL emission region.

3. Morphology of the extended coronal gas

Figure 1 displays the [Fe VII] (left panel) and [Fe X] (right panel) flux distribution found for NGC 3393, evidencing the extension of the coronal gas. It can be seen that this energetic emission is arranged within the bi-cones already mapped by means of the [O III] line. The [Fe VII] emission is detected up to 1.2 kpc NE and 2.2 kpc SW from the AGN. The emission is clearly constrained to an "S" shape structure. To the best of our knowledge, this is the first report of coronal emission detection at kiloparsecs scales in this source. Similarly, the [Fe X] gas is spatially resolved within the "S" feature, coinciding with the most intense region of [Fe VII]. The maximum extension of [Fe X] is found at a distance of 1241 ±152 pc, being identified when integrating the signal in a circle of radius 0.4″.

The results found for the other six sources (not shown here due to space limitations) are very similar to that of NGC 3393. In IC 5063, the coronal gas is found up to 1 kpc NW and 0.9 kpc SE. In NGC 5728, the CL extends up to 2 kpc SE and 1.6 kpc NW. NGC 1068 displays the largest CLR detection, with [Fe VII] found at 2.8 kpc from the AGN. In NGC 5643, [Fe VII] is observed up to 0.8 kpc E and 0.9 kpc W to the AGN. Finally, The Circinus Galaxy and ESO 428-G14 show the most compact (but still rather extended) CLR, observed at ~700 pc from the AGN. To the best of our knowledge, these seven Seyfert 2 display the largest CLR already detected in samples of local AGN.

Figure 1 also evidences that the gas distribution is clumpy. Although the CL emission is the brightest at the AGN position, secondary peaks are also detected along the bi-cones.

The strong relationship between coronal emission, dust extinction and the radio jet is evident in Figure 2. For each galaxy, the left panel is the E(B-V) in mag, determined from the Hα/Hβ ratio. The middle panel is a zoom of the extinction maps around the AGN. The right panel is the [Fe VII] map overlaid to the radio jet contours. It can be seen that, overall, the region where the coronal line is observed displays very little or no extinction while regions outside the coronal region usually display larger values of E(B-V). Moreover, the jet is co-spatial to the coronal gas. We suggest that the passage of the radio jet through the ISM produces shocks that destroy the dust, liberating metals such as iron, allowing the emission of the coronal lines.

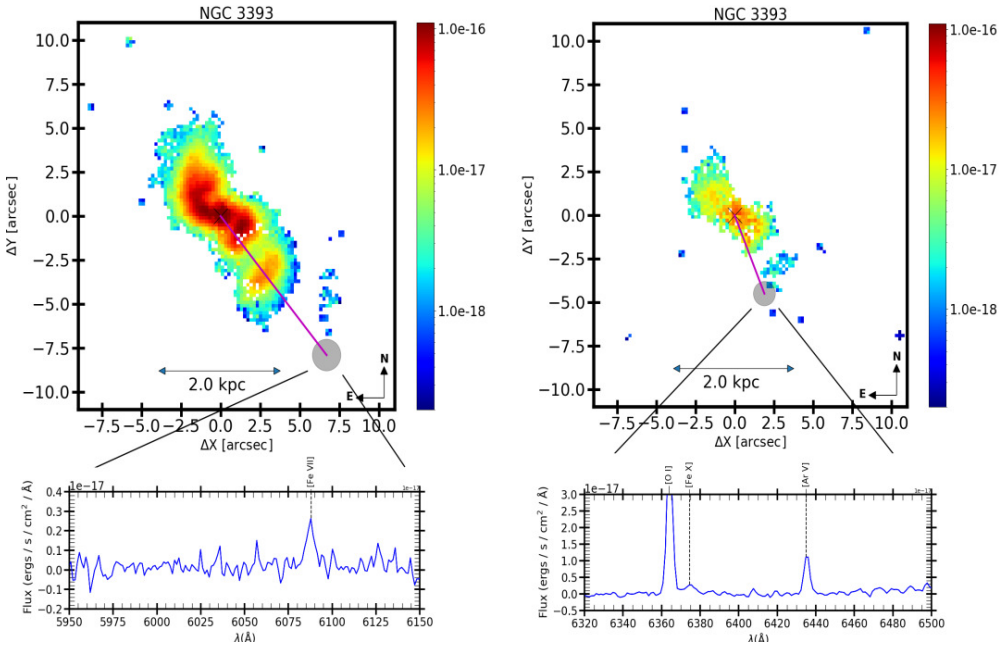


Figure 1. Coronal emission found in NGC 3393. Left: the upper panel shows the [Fe VII] emission. The bottom panel shows the spectrum at the position of the most extended emission, obtained after integrating the signal in the grey circle of radius 0.2″ (top). The magenta line indicates the maximum extension found for [Fe VII] line. Right: similar to the left panel for [Fe X]. The white regions correspond to locations where the lines where not detected or the S/N < 3σ. The colour bars show the fluxes in logarithmic scale and in units of erg s^{-1} cm^{-2} spaxel^{-1}.

Here, we propose that extended coronal emission at projected scales of hundreds of parsecs or a few kpc signals the passage of a radio jet. Shocks induced by the propagation of such a jet through the ISM locally excites the gas, producing the observed coronal line region spectrum.

4. Kinematics of the coronal gas

In order to obtain additional support to the hypothesis that local effects are responsible for the increase in gas ionisation, we study the gas kinematics in the central region of our sample.

To this purpose we employ channel maps, which allow us to examine the velocity field of a spatially distributed gas. This technique consists of slicing a given emission line into velocity bins, so that each bin or channel map shows the regions that simultaneously present a given velocity. Since our main goal is to examine the behaviour of the extended high-ionisation gas, we will use the line of [Fe VII] λ6087 as representative of this gas. In the slicing process, we assume the minimum possible *bin* of the spectra as an interval between the channels. In MUSE spectra, this corresponds to $\Delta\lambda = 1.25$ Å or 61.5 km s^{-1} in velocity space at the position of [Fe VII]. Line fluxes are measured if they are 2σ above the continuum level. The adopted region to measure the standard deviation of the continuum has a width of ∼ 30 Å right before and after the region where the emission line of [Fe VII] is identified.

Figure 3 shows the results found for IC 5063 as a showcase of the sample of AGN studied. Other objects of the sample display a very similar behaviour. We found parcels of coronal gas, mostly close to the radio jet lobes, display the largest offset velocities relative to the systemic (v = 0 km s^{-1}). Indeed, blueshifted gas moving at velocities of ∼600 km s^{-1} is clearly observed. Such region is spatially associated to the NW radio lobe. Similarly, to the SE, redshifted gas at v >350 km s^{-1} is clearly associated to the SE radio lobe.

The channel maps studied for IC 5063 evidences the strong association between coronal emission and the strong turbulence that the jet impacts to that gas, particularly the parcels that are close to the radio lobes.

5. Photionisation models

In the previous sections, we highlighted the presence of highly ionised gas in IC 5063 as we approach the jet's axis, being the highest at the position of the AGN and very close to the radio-lobes, hundreds of parsecs away from the AGN. Indeed, at the NW and SE lobes, the [Fe VII] emission is enhanced, reaching one tenth of its value at the nucleus. A similar result was already reported in Circinus by Fonseca-Faria et al. (2021). They found peaks of [Fe VII] emission of the same order of intensity as that measured in the nucleus, at regions located hundreds of parsecs from the AGN. According to Ferguson et al. (1997), in an scenario dominated by photoionisation by the central source, gas ionisation is expected to decrease with distance. From their models, coronal lines could not be formed at distances greater than 100 pc from the central engine if its $L_{\rm bol}$ is smaller than $10^{43.5}$ erg s^{-1}. This result is still useful in the case of IC 5063, which has a bolometric luminosity a bit larger ($L_{\rm bol} = 10^{44}$ erg s^{-1}). Thus, the evidence gathered here for IC 5063 show that photoionisation by the AGN alone could not explain the kiloparsec size of the CLR in this object. Local excitation mechanisms must likely be producing an increase in gas ionisation along the direction where the [Fe VII] is observed. It is still possible that the presence of gas with very low density ($n_{\rm e} < 50$ cm^{-3}) may explain this result. However, such values of electron density, particularly in the radio lobes or close to them, are not observed (Mingozzi et al. 2019).

In the light of the results gathered here and by other authors, in this section we model the observed emission line spectra in the Circinus Galaxy using the combine effect of photionisation

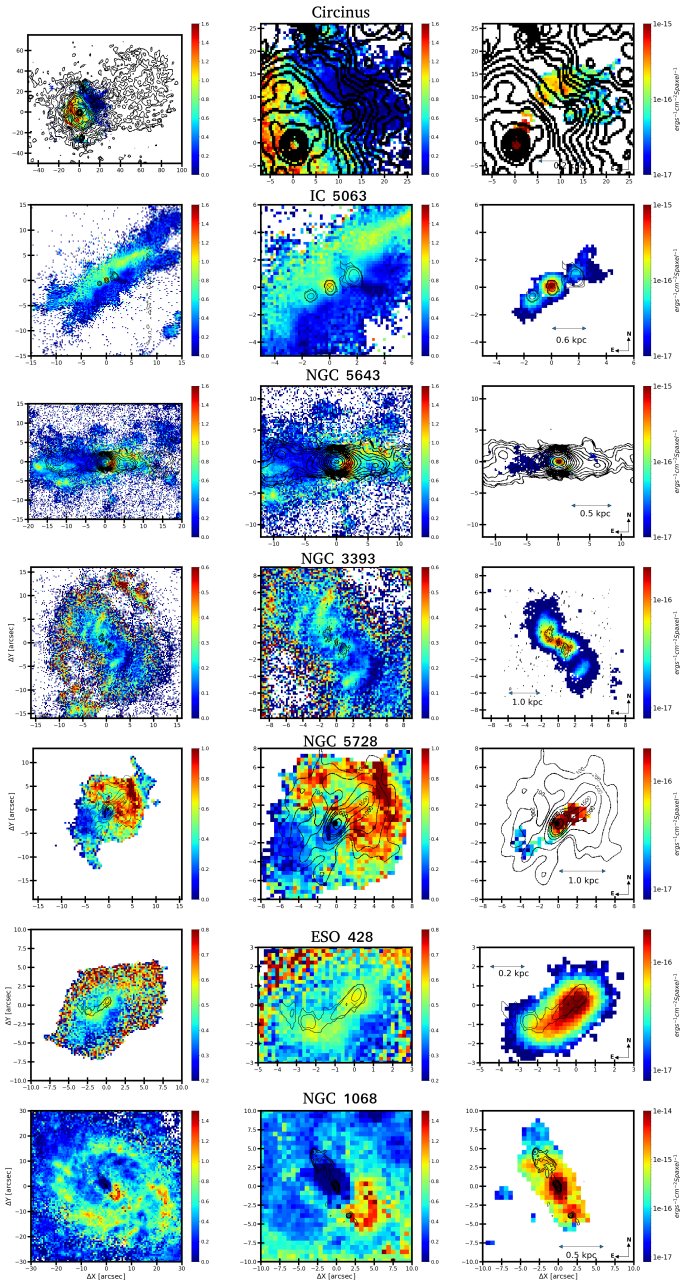


Figure 2. Extinction maps (left), zoom around the AGN position of the extinction maps (middle) and [Fe VII] flux maps (right). The black contours in the latter panels is the radio-emission.

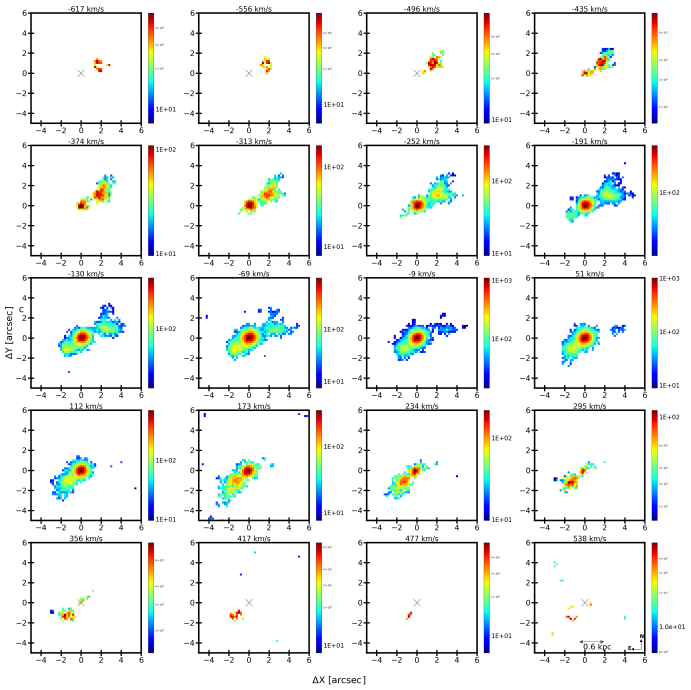


Figure 3. Channel maps of the line of [Fe VII] λ6087 for galaxy IC 5063. Fluxes are presented in units of 10^{-20} erg s^{-1} cm^{-2} spaxel^{-1}. The number at the top of each panel represents the central velocity of the bin.

by the AGN and shocks likely originated by the radio jet. Results for the other galaxies of the sample are in progress.

We have used for the calculation of the predicted line flux ratios the photoionisation code SUMA (Contini & Viegas 2001). As explained in Fonseca-Faria et al. (2021), the main input parameters are those which lead to the calculations of line and continuum fluxes that best matches the observed ones. From the modeling, we found that the maximum temperature reached in the immediate post-shock region $T \sim 1.5{\times}10^5$ $(V_s/100$ km s$^{-1})^2$. T decreases downstream leading to recombination. The cooling rate is calculated in each slab. The line and continuum emitting regions throughout the galaxy cover an ensemble of fragmented clouds. The geometrical thickness D of the clouds is an input parameter which is calculated consistently with the physical conditions and element abundances of the emitting gas. The fractional abundances of the ions are calculated resolving the ionisation equations for each element (H, He, C, N, O, Ne, Mg, Si, S, Ar, Cl, Fe) in each ionisation level. Then, the calculated line ratios, integrated throughout the cloud geometrical width, are compared with the observed ones. The calculation process is repeated changing the input parameters until the observed data are reproduced by the model results, at maximum within 10-20 percent for the strongest line ratios and within 50 percent for the weakest ones.

Using the above approach, we modelled the observed spectra at 12 different regions distributed in the ionisation cone of Circinus. The selected regions are marked in the upper panel of Figure 4 and are overlaid to the [Fe VII] map. The average spectrum of each region was calculated and confronted to the model predictions.

The bottom panel of Figure 4 shows the ratio between the observed and calculated fluxes for the lines shown in the x-axis of the plot. The full red line represents a perfect match between model predictions and observations. The two red dashed-lines are the 1σ deviation. Notice that most lines are within this uncertainty, including the coronal lines.

Throughout the above approach, we derive pre-shock gas densities n_H in the range 100−300 cm^{-3}, gas temperatures of up to $T_e \sim 3 \times 10^4$ K, and shock velocities of ∼400 km s^{-1}. These values are in very agreement to the ones derived from sensitive emission line flux ratios and FWHM of the line profiles. In the cases where coronal lines are observed, the presence of shock-dominated clouds is a requirement for a good match between model and observations.

6. Conclusions

In this work, we study a sample of seven local radio-weak AGN with the purpose of determining the presence of the feedback kinetic channel due to a low-luminosity radio jet. The main results gathered from this work are as follows.

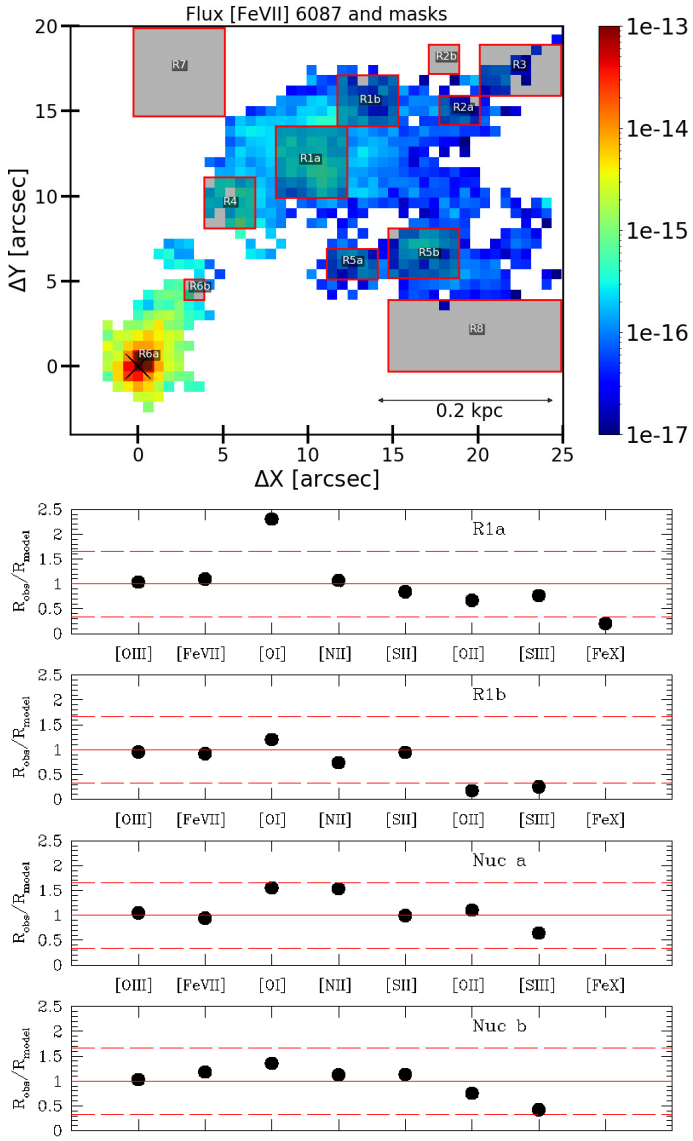


Figure 4. SUMA outputs (bottom panel) for the four selected regions R1a, R1b, Nuc a, and Nuc b, identified in the [Fe VII] map (upper panel). For each region, we give the ratio between model predictions and observation (Y-axis) for different emission lines, normalised to Hβ.

- Extended [Fe VII] emission, at kpc scales, highlights the relevance of the kinetic channel as an important way of depositing energy to the ISM of low-luminosity AGN, even when driven by radiatively poor radio jets.
- The seven sources examined in this work are a showcase of this scenario. We found a conspicuous [Fe VII] emission filling the inner cavities of the ionization cone. It extends up to 2 kpc from the AGN in NGC 3393, NGC 5728 and IC 5063.
- We show that extended coronal emission is associated to the presence of radio jets, lack of dust and extended X-ray emission. The central source plays a fundamental role for gas at distances R < 100-200 pc from the AGN, but at larger R, shocks driven by the jet is fundamental to enhance the coronal emission.
- photoionsation models that combine the effects of shocks and the radiation from a central source were employed to simulate the physical conditions of the gas. Results for the Circinus Galaxy are shown. Twelve representative regions of the nuclear and circumnuclear environment across the FoV covered by MUSE were employed. We found that low- to medium-ionisation lines are mostly produced by radiation dominated clouds, illuminated by the AGN continuum. In contrast, high ionisation lines ([Fe VII] and [Fe X]) are formed in shock dominated clouds. The shock velocities necessary to reproduced the observe spectra are in agreement with that measured from the gas kinematics.

Acknowledgements. The authors thank the Brazilian Agencies: Agency of Coordenação de Aperfeiçoamento de Pessoal de Nível Superior (CAPES), and Conselho Nacional de Desenvolvimento Científico e Tecnológico (CNPq).

References

Appenzeller I., Wagner S. J., 1991, A&A, 250, 57
Bruzual G., Charlot S., 2003, MNRAS, 344, 1000
Cardelli J. A., Clayton G. C., Mathis J. S., 1989, ApJ, 345, 245
Cid Fernandes R., Mateus A., Sodré L., Stasińska G., Gomes J. M., 2005, MNRAS, 358, 363
Contini M., Viegas S. M., 2001, The Astrophysical Journal Supplement Series, 132, 211
Erkens U., Appenzeller I., Wagner S., 1997, A&A, 323, 707
Ferguson J. W., Korista K. T., Ferland G. J., 1997, The Astrophysical Journal Supplement Series, 110, 287
Fonseca-Faria M. A., Rodríguez-Ardila A., Contini M., Reynaldi V., 2021, MNRAS,
May D., Rodríguez-Ardila A., Prieto M. A., Fernández-Ontiveros J. A., Diaz Y., Mazzalay X., 2018, MNRAS, 481, L105
Mazzalay X., Rodríguez-Ardila A., Komossa S., McGregor P. J., 2013, MNRAS, 430, 2411
Mingozzi M., et al., 2019, A&A, 622, A146
Müller-Sánchez F., Prieto M. A., Hicks E. K. S., Vives-Arias H., Davies R. I., Malkan M., Tacconi L. J., Genzel R., 2011, ApJ, 739, 69
Negus J., Comerford J. M., Müller Sánchez F., Barrera-Ballesteros J. K., Drory N., Rembold S. B., Riffel R. A., 2021, ApJ, 920, 62
Prieto M. A., Marco O., Gallimore J., 2005, MNRAS, 364, L28
Ramos Almeida C., Ricci C., 2017, Nature Astronomy, 1, 679
Rodríguez-Ardila A., Fonseca-Faria M. A., 2020, ApJ, 895, L9
Rodríguez-Ardila A., Prieto M. A., Viegas S., Gruenwald R., 2006, ApJ, 653, 1098
Rodríguez-Ardila A., Prieto M. A., Mazzalay X., Fernández-Ontiveros J. A., Luque R., Müller-Sánchez F., 2017, MNRAS, 470, 2845
Speranza G., et al., 2022, A&A, 665, A55
Trindade Falcão A., Kraemer S. B., Crenshaw D. M., Melendez M., Revalski M., Fischer T. C., Schmitt H. R., Turner T. J., 2022, MNRAS, 511, 1420